Solution Structure of Neuronal Bungarotoxin Determined by Two-Dimensional NMR Spectroscopy: Sequence-Specific Assignments, Secondary Structure, and Dimer Formation†

Robert E. Oswald,*,‡,§ Michael J. Sutcliffe,§,∥ Michelle Bamberger,‡,§ Ralph H. Loring,⊥ Emory Braswell,○ and Christopher M. Dobson§

Department of Pharmacology, College of Veterinary Medicine, Cornell University, Ithaca, New York 14853, Inorganic Chemistry Laboratory, University of Oxford, South Parks Road, Oxford OX1 3QR, U.K., Biological NMR Centre, University of Leicester, Leicester LE1 9HN, U.K., Department of Pharmacology, Northeastern University, Boston, Massachusetts 02115, and National Facility for Analytical Ultracentrifugation, University of Connecticut, Storrs, Connecticut 06269

Received December 11, 1990; Revised Manuscript Received February 27, 1991

ABSTRACT: The solution structure of neuronal bungarotoxin (nBgt) has been studied by using two-dimensional ^{1}H NMR spectroscopy. Sequence-specific assignments for over 95% of the backbone resonances and 85% of the side-chain resonances have been made by using a series of two-dimensional spectra at four temperatures. From these assignments over 75% of the NOESY spectrum has been assigned, which has in turn provided 582 distance constraints. Twenty-seven coupling constants (NH–αCH) were determined from the COSY spectra, which have provided dihedral angle constraints. In addition, hydrogen exchange experiments have suggested the probable position of hydrogen bonds. The NOE constraints, dihedral angle constraints, and the rates of amide proton exchange suggest that a triple-stranded antiparallel β sheet is the major component of secondary structure, which includes 25% of the amino acid residues. A number of NOE peaks were observed that were inconsistent with the antiparallel β-sheet structure. Because we have confirmed by sedimentation equilibrium that nBgt exists as a dimer, we have reinterpreted these NOE constraints as intermolecular interactions. These constraints suggest that the dimer consists of a six-stranded antiparallel β sheet (three from each monomer), with residues 55–59 forming the dimer interface.

A group of polypeptide neurotoxins (α-neurotoxins) from the venoms of elapid and hydrophid snakes [e.g., α-bungarotoxin (αBgt)[1]] block synaptic transmission at the vertebrate neuromuscular junction by binding with very high affinity to nicotinic acetylcholine receptors (nAChRs). Of this group of neurotoxins, αBgt, isolated from the venom of *Bungarus multicinctus* native to Taiwan, has been used extensively to study nAChRs from skeletal muscle. nAChRs are nonselective cation channels that are activated by the binding of acetylcholine (ACh), and α-neurotoxins block the functional activity by binding to a site that overlaps the ACh binding site. Neuronal bungarotoxin (nBgt; also known as Bgt 3.1, toxin F, and κ-bungarotoxin) is a minor protein component of the venom of *B. multicinctus* that was originally described as a contaminant of a preparation of αBgt (Ravdin & Berg, 1979), but unlike αBgt, nBgt was shown to block ganglionic nicotinic AChRs with high affinity (Ravdin & Berg, 1979; Chiappinelli, 1983; Loring et al., 1984). Purification and sequencing of this component of the venom revealed that it exhibits considerable sequence homology to other known α-neurotoxins. Recently, three other neuronal α-neurotoxins (κ-flavitoxin, κ_2-bungarotoxin, and κ_3-bungarotoxin; Chiappinelli et al., 1987, 1990) have been isolated from snakes of the genus *Bungarus* that have sequence homologies of 82% or greater with neuronal bungarotoxin and similar biological specificity.

In the peripheral nervous system, nBgt binds with high affinity to two sites, one of which is the same as the αBgt binding site. The site that is unique for nBgt corresponds to a functional nAChR [reviews, Chiappinelli (1984) and Loring and Zigmond (1988)]. This has led to the use of nBgt as a probe for neuronal nAChRs in the peripheral nervous system. With the recent cloning of cDNA corresponding to neuronal nAChRs, the functional nAChR that binds nBgt but not αBgt has been characterized in some detail. The receptor subtype with the highest affinity for nBgt consists of two gene products that have sequence homologies to subunits of the skeletal muscle nAChR and that comprise the subunits of the neuronal nAChR. These subunits are (1) α_3, which contains the ACh

† This work was supported by grants from the National Institutes of Health (R01 NS18660 and a senior fellowship), the Fulbright Foundation, and the Cornell Biotechnology Institute to R.E.O., the National Institutes of Health (NS22472) to R.H.L., and the National Science Foundation (DIR 8717034) to E.B. C.M.D. is a member of the Oxford Centre for Molecular Sciences, and M.J.S. is a Royal Society University Research Fellow.

* Address correspondence to this author.
‡ Cornell University.
§ University of Oxford.
∥ University of Leicester.
⊥ Northeastern University.
○ University of Connecticut.

[1] AMX, a three-spin system for which the chemical shift differences are greater than the coupling constants; αBgt, α-bungarotoxin; ACh, acetylcholine; *B*, second virial coefficient; COSY, two-dimensional *J*-correlated spectroscopy; $d_{\alpha N}$, NOE connectivity between the backbone NH proton and the αCH proton of the previous residue; $d_{\beta N}$, NOE connectivity between the backbone NH proton and the βCH proton of the previous residue; DOUBLE RELAY, two-dimensional double-relayed *J*-correlated spectroscopy; d_{NN} NOE connectivity between the backbone NH proton and the NH proton of the previous residue; HOHAHA, two-dimensional homonuclear Hartmann–Hahn spectroscopy; nAChR, nicotinic acetylcholine receptor; nBgt, neuronal bungarotoxin; NMR, nuclear magnetic resonance; NOE, nuclear Overhauser effect; NOESY, two-dimensional NOE spectroscopy; ω_1, Fourier transform of t_1 dimension; ω_2, Fourier transform of t_2 dimension; RELAY, two-dimensional relayed *J*-correlated spectroscopy; TOCSY, two-dimensional total correlation spectroscopy; t_1, evolution time; t_2, data acquisition time.

0006-2960/91/0430-4901$02.50/0

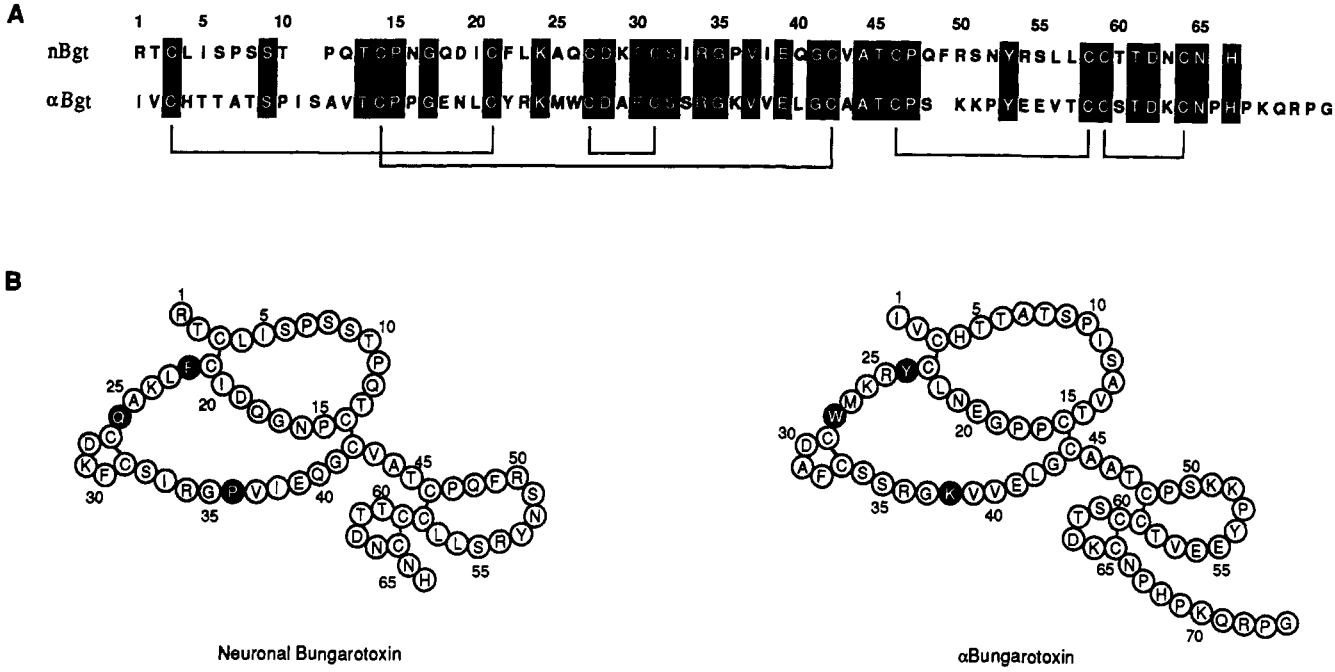

FIGURE 1: Comparison of nBgt with αBgt. (A) Sequence alignment of nBgt and αBgt. nBgt and αBgt exhibit a considerable degree of sequence homology and an identical disulfide bonding pattern. The identical residues comprising 47% of nBgt are indicated with a black background, and nBgt numbering is used. (B) Schematic representation of the two toxins, with important differences between the two proteins indicated with a black background. Sequence information was obtained as follows: nBgt (Grant & Chiappinelli, 1985; Loring et al., 1986) and αBgt (Ohta et al., 1987; Kosen et al., 1988).

binding site, and (2) β_2, which is a homologous protein that is required to form a functional receptor (Boulter et al., 1987). Interestingly, a receptor formed from a homologous β subunit (β_4) and the α_3 subunit is a functional ion channel but is not blocked by nBgt (Duvoisin et al., 1989). This suggests that although nBgt does bind to a portion of the α_3 subunit (McLane et al., 1990), contacts with other portions of this multisubunit protein are also important.

nBgt and related neuronal α-neurotoxins exhibit a number of important sequence differences from α-neurotoxins specific for skeletal muscle nAChRs (Figure 1): (1)Tryptophan 28, of, for example, αBgt is present in all homologous long and short neurotoxins but is not conserved in neuronal α-neurotoxins; (2) neuronal α-neurotoxins are the only long or short neurotoxins to have a proline residue next to a highly conserved arginine–glycine pair (Pro-36 in nBgt); and (3) the conserved tyrosine present in all other α-neurotoxins is substituted by a phenylalanine in the neuronal α-neurotoxins (Phe-22 in nBgt). In addition to these sequence differences, nBgt and other neuronal α-neurotoxins can exist as dimers in solution (unlike most other long α-neurotoxins, which are monomers in solution), which may also be related to their physiological activity (Chiappinelli & Lee, 1985), although some evidence suggests that the monomeric form may by physiologically active (Halvorsen & Berg, 1987). The crystal structures of several α-neurotoxins are known (Low et al., 1976; Tsernoglou & Petsko, 1976; Walkinshaw et al., 1980; Love & Stroud, 1986), and some aspects of the solution structures of α-Bgt (Basus et al., 1988; Endo et al., 1981; Inagaki et al., 1985) and a variety of other α-neurotoxins [e.g., Labhardt et al. (1988)] have been reported. In order to begin to relate the differences between nBgt and other neurotoxins to the differences in function, a knowledge of the three-dimensional structure of nBgt is important.

In this paper, we present the sequence-specific NMR assignments of the proton resonances of nBgt. Greater than 95% of the backbone resonances and 85% of the side-chain resonances have been assigned to specific protons. This has provided us with 106 sequential, 26 medium-range, 39 long-range backbone, and 304 long-range NOE assignments for the nBgt monomer (Wüthrich, 1986). The NOE constraints along with dihedral angle constraints, amide proton exchange rates, and the position of disulfide bonds suggest that nBgt has a three-loop structure and a triple-stranded antiparallel β sheet similar to other snake α-neurotoxins. In addition, the NOE distances (12 long-range backbone intermolecular assignments) and amide exchange rates indicate the position of the dimer interface, which in turn predicts an intermolecular six-stranded antiparallel β sheet.

Materials and Methods

Purification of Neuronal Bungarotoxin. nBgt was purified as described previously (Loring et al., 1986). Fractions from the venom of *B. multicinctus*, purchased from Biotoxins, Inc. (St. Cloud, FL), were dialyzed and purified by preparative isoelectric focusing on Sephadex G-50 superfine. After elution, the protein was dialyzed against 0.1 M ammonium acetate and purified further on a CM-cellulose column (0.1–0.3 M ammonium acetate gradient, pH 5.0–7.4). The purified toxin was assayed for activity by measuring the blockade of nicotinic transmission in the chick ciliary ganglion (Chiappinelli & Zigmond, 1978) and for purity by analytical isoelectric focusing, $NaDodSO_4$–polyacrylamide gel electrophoresis (Loring et al., 1984), and gas-phase sequencing (Loring et al., 1986). For the NMR experiments, 15 mg of the toxin was lyophilized, resuspended in 0.5 mL of 0.02% sodium azide, and titrated to pH 4.2 with HCl. The final concentration of nBgt was 4 mM. Several experiments were performed at a concentration of 8 mM nBgt. The additional 15 mg of purified nBgt was supplied by Biotoxins, Inc.

NMR Spectroscopy. Most NMR spectra were recorded either at 600.13 MHz on a Bruker AM-600 spectrometer, at 500.1 MHz on a Bruker AM-500 spectrometer, or at 500.1 MHz on a laboratory-built GE-Nicolet spectrometer (Oxford Centre for Molecular Sciences). In addition, several experiments were performed at Syracuse University (NIH Resource

for Multinuclear NMR and Data Processing; GE500 spectrometer) and at the University of Leicester (Biological NMR Centre; Bruker AMX-600 spectrometer). To resolve spectral overlap, data were collected at temperatures of 14, 27, 37, and 42 °C in H_2O (i.e., 90% H_2O and 10% D_2O) and D_2O. All spectra were acquired in the phase-sensitive mode by using the procedure of States et al. (1982) on the GE spectrometers and by using time-proportional phase incrementation (Marion & Wüthrich, 1983) on the Bruker spectrometers. Spectral widths ranged from 5208 to 8064 Hz in both dimensions with the carrier set on the water resonance. The decoupler was set on the water resonance except for some experiments in D_2O, for which the decoupler was cycled between the residual water resonance and a contaminating acetate resonance. With this cycling procedure, we were able to use a higher gain setting, which in turn increased the sensitivity. For NOESY (Jeener et al., 1979; Kumar et al., 1980; mixing times between 25 and 300 ms) and HOHAHA (MLEV-17 sequence; Bax & Davis, 1985; mixing times between 32 and 72 ms) experiments, 256 complex increments in t_1 (96–128 scans per increment) and 1024 complex data points in t_2 were recorded. For COSY (Aue et al., 1976; Bax & Freeman, 1981) and related experiments (RELAY, DOUBLE RELAY; Eich et al., 1982; Bax & Drobny, 1985), 512 complex increments in t_1 (32–64 scans per increment) and 1024 complex data points in t_2 were recorded. In both cases, data were zero filled to 2048 complex points in both dimensions before Fourier transformation, resulting in a 2K × 2K real matrix. In some cases, a pre-TOCSY sequence was used in the NOESY or COSY experiment to recover magnetization lost by saturation of the H_2O resonance (Otting & Wüthrich, 1987). For spectra collected on the Bruker spectrometers, the time domain signal was multiplied by a sine bell function shifted by 3° before transformation (Wagner et al., 1978). For the GE-Nicolet data, the resolution was enhanced by trapezoidal modification and double-exponential modification in t_2 and trapezoidal modification only in t_1 (Redfield & Dobson, 1988). In some cases, the NOESY and HOHAHA spectra were multiplied by a $\cos^2$ window to increase the signal-to-noise ratio (Kline et al., 1988). The data were processed either with Bruker software or with FTNMR (Hare Research, Inc) running on either a MicroVAX II computer or a Sun 4 computer. In some cases, the residual H_2O resonance was removed from the spectrum by a repetitive use in the time domain of a three-point smoothing routine (SM3 in FTNMR) followed by subtraction of the smoothed spectrum from the original spectrum. This effectively removed the t_1 noise associated with the residual H_2O resonance. All spectra are shown as contour plots. Positive and negative contours are shown for COSY and related experiments, and only the positive levels are shown for NOESY and HOHAHA spectra. The contour levels are spaced geometrically (1.4 times the previous level determines the next level). The horizontal and vertical axes represent ω_2 and ω_1, respectively.

Measurements of Coupling Constants. For measurements of NH–αCH coupling constants, COSY spectra were collected with 8192 complex points in t_2 with a spectral width of 5618 Hz. The records were zero filled once and transformed in the t_2 dimension, resulting in a resolution in ω_2 of 0.34 Hz/point. Only the portions of the spectrum corresponding to the fingerprint region were transformed in t_1. Cross sections through each NH–αCH peak were extracted from the 2D spectrum (two antiphase pairs) and used for further analysis. The coupling constants were determined by simulating the cross peak, taking into account the spectral resolution and resolution enhancement. The residual sum of squared deviations from the experimental data (i.e., the antiphase pair) were minimized by using the Simplex algorithm (Press et al., 1986) as described by Redfield and Dobson (1990). In this way, and accurate value of the coupling constant independent of the line width could be determined. Dihedral constraints for the main-chain dihedral angle ϕ were determined from NH–αCH coupling constants greater than 8 Hz or less than 5 Hz by using the Karplus equation (Pardi et al., 1984). All computations were performed on a MicroVAX II computer.

Measurements of Hydrogen Exchange. Qualitative measurements of hydrogen exchange were made by freshly dissolving the sample in D_2O and performing pre-TOCSY COSY experiments at 0.75, 1.5, 8.5, 22.5, 48, 72, and 216 h. The initial four experiments were performed with 2 scans per increment with only minimal phase cycling. All NH–αCH cross peaks observed with 48 scans per increment could be observed with 2 scans per increment. Rapidly exchanging amide protons were defined as those for which an NH–αCH cross peak could not be observed at 0.75 h, intermediate exchange was defined as those lost by 22.5 h, and slowly exchanging protons were still present at 216 h.

Sedimentation Equilibrium. The sedimentation equilibrium experiments were performed in order to ascertain whether nBgt exists in solution as a monomer or dimer under the conditions used in this study. The results were analyzed essentially as described by Yphantis and Arakawa (1987) except that the "short column" technique was not used. Three concentrations (0.1, 0.3, and 1 mg/mL) of the protein solution (in 0.02% NaN_3 at pH 4.2) were centrifuged at 28 000 rpm and 20 °C in 30-mm six-channel exterior loading cells. Sedimentation equilibrium was achieved in 18–24 h, and the data were recorded photographically. In a similar manner, data were obtained from protein solutions (concentrations of 0.04, 0.1, and 0.3 mg/mL) that had been centrifuged at 44 000 rpm until equilibrium had been attained.

The data analysis yields a best fit for various assumed molecular models. The analysis was performed simultaneously on the six sets of data obtained from the two sedimentation experiments performed at the two speeds. The concentration range (resulting largely from the centrifugal effect) of the data was from a few micrograms per milliliter to approximately 2 mg/mL. Each attempted fit results in a value (σ) that is proportional to the weighted average molecular weight (M_w) of the molecule and a value of B (the second virial coefficient) for a nonassociating model. For an associating model, the analysis yields the value of σ for the associating monomer and the equilibrium constant. In both cases, the rms error and a graph of residual errors is produced to provide information regarding the quality of the fit. The molecular weight was calculated from σ by using the specific volume ($\bar{v}$ = 0.717 mL/g) determined from the amino acid composition (Cohn & Edsall, 1943) and the density of the solvent (0.99835 g/mL at 20 °C) determined with a Paar DMA 602 density meter.

Results

The fingerprint region of the 500-MHz COSY spectrum of nBgt at 37 °C in H_2O is shown in Figure 2A. The NH–αCH cross peaks were identified by using the two-stage procedure described by Wüthrich (1986), which consists of the analysis of spin systems followed by sequential assignments.

Analysis of Spin Systems. For the most part, the assignment of spin systems was performed by using the COSY, RELAY, DOUBLE RELAY, NOESY, and HOHAHA experiments in D_2O and H_2O. nBgt is composed of 66 amino acid residues, including five prolines and three glycines. All

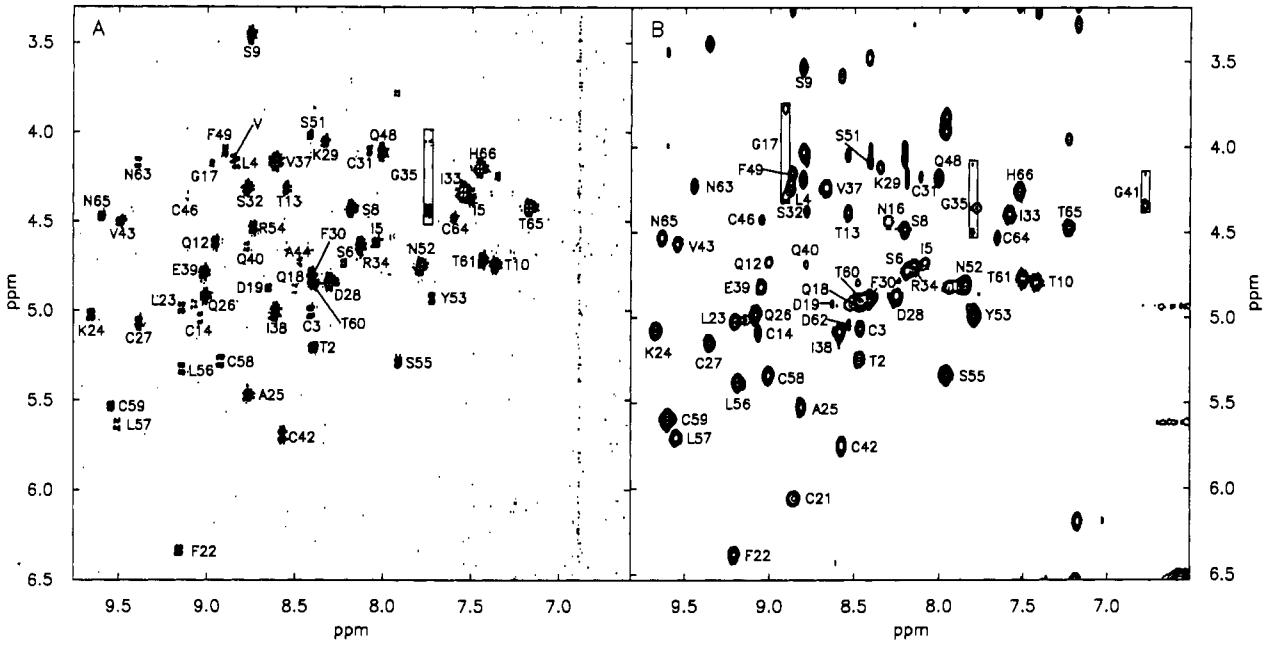

FIGURE 2: Spectra showing the fingerprint region of nBgt. (A) A phase-sensitive pre-TOCSY COSY spectrum obtained with 4 mM nBgt at 500 MHz at 37 °C in 90% H_2O/10% D_2O is shown. The data were processed by using FTNMR with a sine bell window function shifted by 3° in both dimensions. (B) A HOHAHA spectrum collected in 90% H_2O/10% D_2O with 8 mM nBgt at 600 MHz and 42 °C is shown. The data were processed by using FTNMR with a $\cos^2$ window function in both dimensions. All three glycines are clearly present in this spectrum.

of the 63 expected NH–αCH cross peaks have been identified; however, several additional low-intensity peaks are present in the fingerprint region. This suggests either that a small contaminant is present in the preparation or that more than one form of the toxin exists in solution (e.g., monomer and dimer). For α protons resonating close to the saturated H_2O protons, a pre-TOCSY sequence was used to recover the magnetization.

Of the three glycine residues, NH–αCH cross peaks of only one (Gly-35) could be unambiguously identified in COSY spectra recorded at 4 mM in H_2O by its characteristic fine structure (Figure 2A). The NH–αCH cross peaks of Gly-41 were detected in a double-quantum-filtered COSY spectrum recorded in D_2O with a double saturation of the residual HDO and contaminating acetate resonances. This procedure allowed the use of a higher gain setting, providing an increase in sensitivity. As discussed below, the slow exchange of the amide proton of Gly-41 is consistent with a hydrogen bond within a β sheet. Gly-17 was not observable at 4 mM nBgt but was faintly present in a COSY spectrum at 8 mM nBgt (42 °C). A HOHAHA spectrum in H_2O (Bruker AMX-600; 8 mM, 42 °C) clearly revealed the spin systems for all three glycines (Figure 2B).

The aromatic protons of the tyrosine residue and the three phenylalanine residues could be identified easily (Figure 3). The chemical shift of the 4-proton of Phe-22 was shifted downfield relative to the 3,5-protons, but the spin system was readily distinguished from that of tyrosine by the RELAY and HOHAHA spectra. On the other hand, the 4-proton of Phe-49 was shifted upfield relative to the 4,6-protons but again was identified with the RELAY and HOHAHA spectra. The α and β protons of tyrosine and phenylalanine form an AMX system with a characteristic coupling pattern. The AMX system corresponding to the aromatic protons was identified by strong NOE cross peaks between the β protons (and sometimes α protons) and the 3,5-protons of tyrosine or phenylalanine (Wüthrich, 1986).

The two lysines and three of the four arginines could be identified by using both the HOHAHA and the COSY

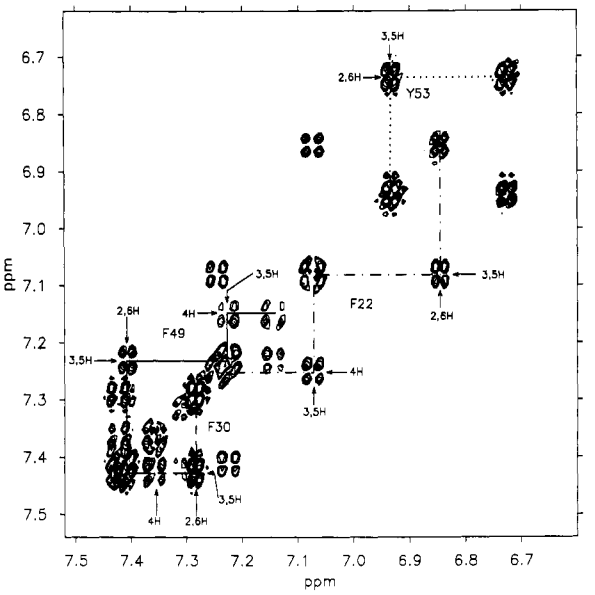

FIGURE 3: Double-quantum-filtered COSY spectrum of nBgt obtained at 600 MHz and 42 °C in D_2O showing the cross peaks arising from protons on aromatic side chains. The data were processed by using FTNMR with a sine bell window function shifted by 3° in both dimensions. The assignment of Phe-20 was confirmed by RELAY and HOHAHA spectra.

spectra. In each case, connectivities from the side-chain amide protons could be traced by using relay peaks in the HOHAHA spectrum from the ϵCH to the δCH, γCH, and βCH. In most cases, relay peaks between the backbone NH and the βCH, γCH, and δCH could also be observed. Side-chain amides for glutamine and asparagine were identified where possible by NOE connectivities between the amide protons and the γCH or βCH protons, respectively.

The six threonine, two valine, and two alanine residues could be identified readily from COSY and RELAY spectra and, in the case of valine and threonine, DOUBLE RELAY spectra. In the cases of Thr-61 and Thr-10, the αCH–βCH cross peaks could only be observed in D_2O spectra, but the

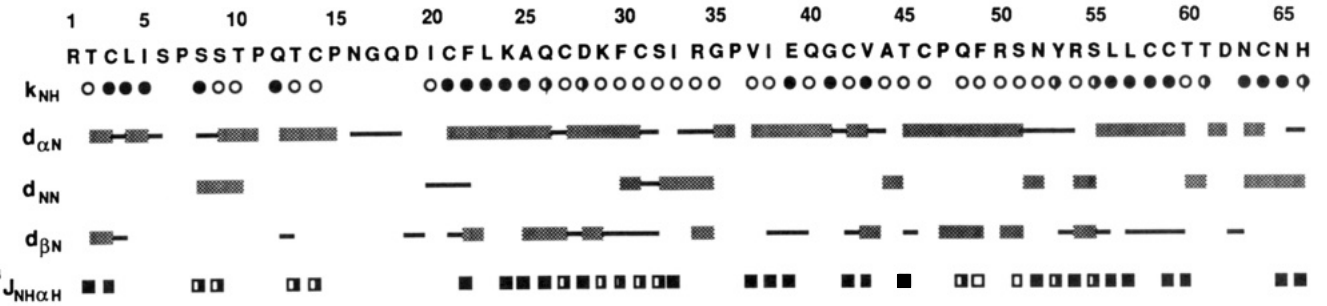

FIGURE 4: Amino acid sequence and summary of sequential NOE connectivities, coupling constants, and amide exchange rates. The sequential connectivities giving rise to strong NOE peaks are shown with the shaded band and those giving rise to weak NOE peaks with the solid line ($d_{\alpha N}$, d_{NN}, $d_{\beta N}$). The amide exchange rates (k_{NH}) are represented as slow (●; $<10^{-5}$ min^{-1}), intermediate (◑), or fast (○; $>10^{-2}$ min^{-1}). The coupling constants ($^3J_{NH\alpha H}$) are represented as <5 Hz (□), between 5 and 8 Hz (◨), or >8 Hz (■).

Table I: Chemical Shifts of the Assigned ^{1}H Resonances in Neuronal Bungarotoxin (37 °C)

residue	NH	αH	βH	others	residue	NH	αH	βH	others
Arg-1					Gly-35	7.720	4.01, 4.4		
Thr-2	8.350	5.170	3.780	γCH_3 1.10	Pro-36			2.79, 2.96	γCH_2 1.835, 1.91; δCH_2 3.51, 3.71
Cys-3	8.380	4.980	2.55, 2.88						
Leu-4	8.800	4.140	1.410	γCH 1.315; δCH_3 0.475, 0.58	Val-37	8.580	4.140	2.030	γCH_3 0.94, 1.04
Ile-5	8.010	4.610	1.940	γCH_2 1.51, 1.38; γCH_3 1.09; δCH_3 0.76	Ile-38	8.595	4.975	1.795	γCH_2 1.2, 1.4; γCH_3 0.69; δCH_3 0.73
Ser-6	8.200	4.740	4.14, 4.21		Glu-39	9.010	4.740	1.925, 2.07	γCH_2 2.27, 2.36
Pro-7					Gln-40	8.765	4.610		
Ser-8	8.160	4.410	3.940		Gly-41	6.660	4.06, 4.27		
Ser-9	8.725	3.435	3.955, 4.105		Cys-42	8.540	5.660	3.06, 3.515	
Thr-10	7.340	4.710	4.120	γCH_3 1.17	Val-43	9.460	4.490	2.235	γCH_3 0.69, 0.795
Pro-11			1.900	γCH_2 1.695, 2.01; δCH_2 3.605, 3.70	Ala-44	8.470	4.685	1.470	
					Thr-45	7.150	4.390	3.870	γCH_3 1.13
Gln-12	8.920	4.590	1.82, 2.05	γCH_2 2.345, 2.44; ϵNH_2 6.795, 7.29	Cys-46	9.110	4.330	2.305, 2.89	
					Pro-47		4.250	1.78, 2.29	γCH_2 1.35, 1.51; δCH_2 3.33, 3.71
Thr-13	8.530	4.290	3.960	γCH_3 1.27					
Cys-14	9.025	5.010	2.755, 3.435		Gln-48	8.010	4.085	1.88, 2.37	
Pro-15				γCH_2 2.01; δCH_2 3.43, 3.955	Phe-49	8.882	4.085	3.110	2,6H 7.37; 3,5H 7.175; 4H 7.1
Asn-16	8.200	4.370	2.70						
Gly-17	8.880	3.70, 4.24			Arg-50	5.020	4.345	0.175, 1.45	γCH_2 1.16, 1.235; δCH_2 2.975; ϵNH 6.955
Gln-18	8.475	4.840							
Asp-19	8.635	4.830	2.82, 3.39		Ser-51	8.395	4.01	3.695, 3.776	
Ile-20	7.470	4.340	1.940	γCH_2 0.94, 1.01	Asn-52	7.770	4.710	2.615, 3.09	δNH_2 6.67, 7.535
Cys-21	8.800	5.980	2.94, 3.05		Tyr-53	7.695	4.900	2.695	2,6H 6.69; 3,5H 6.895
Phe-22	9.130	6.300	2.725, 3.145	2,6H 6.805; 3,5H 7.025; 4H 7.19	Arg-54	8.710	4.510	1.695, 2.195	δCH_2 3.07, 3.15; ϵNH 7.36
Leu-23	9.110	4.955	1.545	γCH 1.36; δCH_3 0.63, 0.70					
Lys-24	9.640	5.020	1.54, 1.73	γCH_2 0.82, 0.96; δCH_2 1.15; ϵCH_2 2.555	Ser-55	7.895	5.250	3.745, 3.84	
					Leu-56	9.115	5.295	1.74, 2.305	γCH 1.71; δCH_3 1.21, 0.97
Ala-25	8.740	5.430	1.220						
Gln-26	8.980	4.880	1.98, 2.225	γCH_2 2.30	Leu-57	9.490	5.600	1.56, 1.84	γCH 1.095; δCH_3 0.89
Cys-27	9.375	5.080	2.97, 3.30		Cys-58	8.890	5.245	2.34, 2.61	
Asp-28	8.290	4.800	2.80, 3.06		Cys-59	9.515	5.505	3.34, 3.94	
Lys-29	8.305	4.030	1.44, 1.61	γCH_2 0.77, 0.98; δCH_2 1.44; ϵCH_2 2.80; ζNH_2 7.42	Thr-60	8.360	4.815	4.965	γCH_3 1.46
					Thr-61	7.410	4.675	4.240	γCH_3 1.18
Phe-30	8.385	4.775	3.02, 3.40	2,6H 7.24; 3,5H 7.38; 4H 7.315	Asp-62	8.535	4.965	2.440	
Cys-31	8.045	4.080	3.205, 3.575		Asn-63	9.360	4.150	2.73, 2.9	δNH_2 6.19, 7.16
Ser-32	8.750	4.290	3.995		Cys-64	7.580	4.450	3.31, 3.755	
Ile-33	7.520	4.305	1.915	γCH_2 1.265, 1.56; γCH_3 0.97; δCH_3 0.915	Asn-65	9.570	4.445	2.12, 2.43	
					His-66	7.425	4.180	2.775, 3.09	δCH 8.51, 7.42
Arg-34	8.105	4.610	1.93, 2.14	γCH_2 1.645, 1.73; δCH_2 3.1, 3.19; ϵNH 7.10					

NH–βCH RELAY peaks were present both in H_2O and D_2O. A third valine (labeled V in Figure 2A) was observed with low intensity in COSY, RELAY, and DOUBLE RELAY spectra that could not be sequentially assigned (nBgt has only two valine residues). Since one of the valine residues (Val-37) is next to a proline (Pro-36), this system could be a reflection of a minor species containing a cis Gly-35–Pro-36 peptide bond (Chazin et al., 1989; Evans et al., 1989). This is supported by the observation that the chemical shifts of all of the protons in this spin system except the NH are within 0.03 ppm of the corresponding protons in Val-37. Proline residues were not completely assigned in all cases. In most cases, the δH proton and its connectivity to the NH of the following residue could be observed. Except for Pro-47, the αH protons were not assignable from the spectra that we obtained.

Sequential Assignments. The second step of the assignment procedure involved correlating cross peaks in the fingerprint region of the COSY spectrum with specific amino acids in the protein sequence by using d_{NN}, $d_{\alpha N}$, and $d_{\beta N}$ connectivities (derived from the NOESY spectrum) and the spin system assignments (Wüthrich, 1986). The overall assignment strategy is summarized in Figure 4 and Table I. In most cases, the sequential assignment was based on the presence of an NOE cross peak between an α proton resonance and an amide proton resonance for which a scalar coupling does not exist. By use of the spin system assignments and the αH–NH connectivities, the sequential assignments were made. An example of the sequential assignment procedure is illustrated in Figure

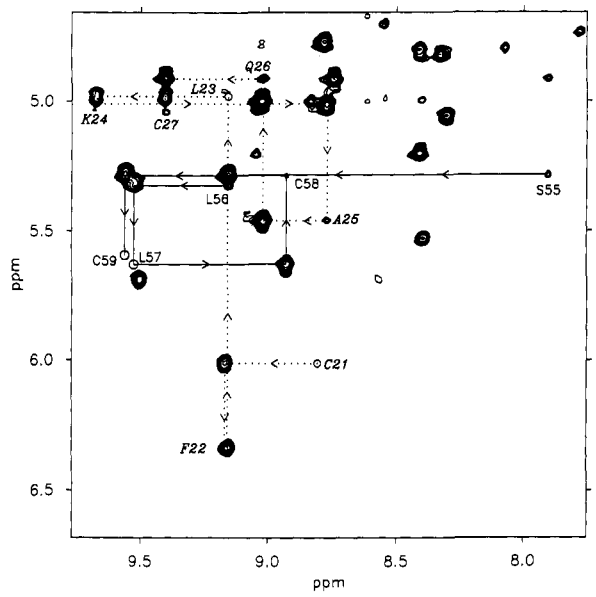

FIGURE 5: Example of the sequence specific assignment of nBgt. Shown here is the fingerprint region of a pre-TOCSY NOESY spectrum of nBgt collected at 500 MHz and 37 °C in 90% H_2O/10% D_2O. The data were processed by using FTNMR with a $\cos^2$ window function in both dimensions. Sequential connectivities between residues 21 and 27 and between residues 55 and 59 are indicated. The positions of the intraresidue NH–αCH cross peaks were determined from the corresponding COSY spectrum and are labeled. If a corresponding NOESY peak is not present, it has been indicated by an open circle.

5 for residues 21–27 and residues 55–59. Interruptions in the chain of assignments occurred at all but one of the proline–X bonds (Pro-47) due to difficulties in the assignment of the proline α protons. Residues 2–5, 8–15, and 20–66 were assigned on the basis of spectra recorded at 4 mM nBgt. The remaining assignments required spectra collected at 8 mM, largely as a result of the identification of Gly-17.

Sedimentation Equilibrium. The model corresponding to a single species best described the data and resulted in a M_w of 14 000 ± 200 and a degree of nonideality (second viral coefficient) of 0.084 ± 0.004 L·mol/g^2. The resulting rms error was small (0.017 fringe, approximately that expected from reading the photographic data) and the residuals exhibited no significant systematic error. The positive value of the second viral coefficient indicated the presence of a small amount of charge. Upon correction of the molecular weight for this effect (Braswell, 1968), the final M_w for the protein was 14 000 ± 200, indicating that the molecule is present under these conditions as a dimer (calculated molecular weight of 14 626). Based on the value of B, the calculated effective charge on the dimer is between 3 and 4.

Secondary Structure. Homologous α-neurotoxins such as αBgt (Love & Stroud, 1986; Bassus et al., 1988) and α-cobratoxin (Walkinshaw et al., 1980) exhibit a triple-stranded antiparallel β sheet. A considerable amount of β-sheet structure is suggested by the downfield-shifted α protons observed both in H_2O and D_2O and the αCH–αCH NOE connectivities. Inspection of the αCH–αCH, NH–NH, and nonsequential αCH–NH NOE connectivities indicates that a triple-stranded antiparallel β sheet is present (Figure 6A). By alignment of nBgt with αBgt according to homologous residues, it is apparent that the secondary structure is almost identical with that observed for αBgt in solution (Figure 6B; Love & Stroud, 1986; Basus et al., 1989). However, a number of NOE connectivities were present that are not consistent with a triple-stranded antiparallel β sheet. These included, among others, NOE connectivities between the αCH of Ser-55 and

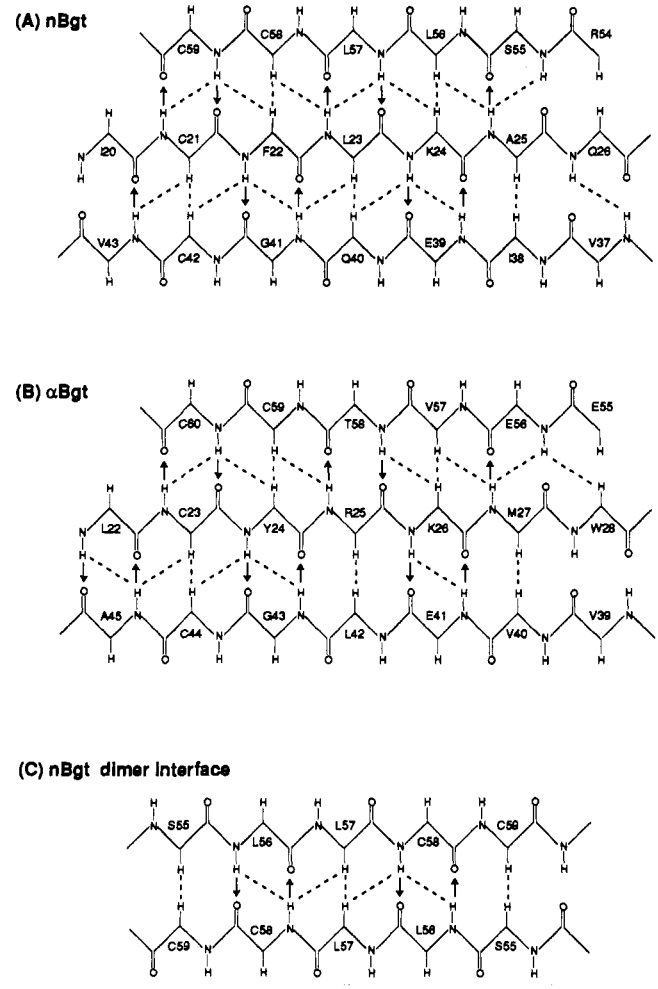

FIGURE 6: Schematic representation of the β-sheet structure of (A) the nBgt monomer, based on the NOE constraints and hydrogen exchange rates from the present study, (B) αBgt, based on the NOE constraints reported by Basus et al. (1988), and (C) the dimer interface of nBgt, based on the NOE constraints and by hydrogen exchange rates that are inconsistent with an intramolecular β sheet. The arrows indicate the position of probable hydrogen bonds, and the dashed lines indicate NOE connectivities. Only the backbone NOE connectivities are shown. The NOE constraints shown in (A) are selected to remove presumed dimer contacts, whereas in (C), the constraints are those presumed to be dimer contacts. All observed NOE constraints are included in (B) (Basus et al., 1988).

the αCH of Cys-59, and between the NH of Leu-56 and the αCH of Leu-57, and between the NH of Leu-56 and the NH of Cys-58. The 1D and 2D spectra of nBgt have line widths similar to those of the spectra obtained with αBgt, which exists as a monomer in solution. Despite this fact, nBgt has been reported to be a dimer in solution (Chiappinelli & Lee, 1985). Since we have shown that nBgt is a dimer under the conditions used in the present study, a viable explanation for the aberrant NOE connectivities is that they represent intermolecular connectivities. As shown in Figure 6C, these connectivities are consistent with an intermolecular antiparallel β sheet. This would suggest that the dimeric structure of nBgt consists of a six-stranded antiparallel β sheet. The similar line widths observed in nBgt and αBgt may be a reflection of some degree of segmental motion within the dimeric structure.

Hydrogen Exchange. Qualitative estimates of backbone amide proton exchange rates were measured by using COSY spectra after freshly dissolving the native protein in a D_2O solution. A summary of the exchange rates is given in Figure 4. Only those rates that could be unambiguously determined are indicated in the figure. Of particular interest are the

exchange rates for the amide protons for residues 21–25, 38–43, and 55–59. These are the residues that form the triple-stranded antiparallel β sheet suggested by the NOE connectivities and by the structure of αBgt. For such a secondary structure, the middle strand would be expected to have amide protons with slow exchange rates, with the outer two strands having residues with exchange rates alternating between fast and slow on the sequence. This arises from the fact that alternate residues have amide protons involved in hydrogen bonds. The amide protons from the presumed middle strand (Cys-21–Gln-26) all have slow exchange rates, and one of the outer strands (Ile-38–Cys-43) exhibits alternating fast and slow rates. The other outer strand (Ser-55–Cys-59), however, consists of backbone amide protons all having slow exchange rates. This suggests that additional hydrogen bonds may exist for the amide protons of Cys-58 and Leu-56. As discussed above, this is consistent with the NOE distances, which suggest that the dimer interface occurs at this segment of the protein. This would indicate that the hydrogen bonds implied by the slow exchange rates for Leu-56 and Cys-58 are intermolecular.

Coupling Constants. Where possible, the coupling constants were measured by comparison of the experimental data with a simulation of the spectrum taking into consideration the window function used to process the data, the line width, the amplitude, and the coupling constant. The summary of the results from this analysis is given in Figure 4. Only those peaks for which adequate signal-to-noise could be obtained were analyzed. As would be expected for a protein with considerable β-sheet structure, a large proportion of the coupling constants were greater than eight, suggesting main-chain ϕ angles characteristic of β sheet.

Discussion

Postsynaptic α-neurotoxins are generally classified as "short" and "long", with short toxins having four disulfide bridges and 60–64 amino acid residues and long toxins having five disulfide bridges and 70–74 residues [for review, see Karlsson (1979)]. The disulfide bonding pattern of nBgt is characteristic of long α-neurotoxins, but it has fewer amino acid residues (66) than other members of the family (with the exception of *Laticauda semifasciata* III α-neurotoxin, which also has five disulfide bridges and 66 amino acids). The studies described here demonstrate that nBgt exhibits an overall folding pattern similar to those of other long and short snake α-neurotoxins (Low et al., 1976; Tsernoglou & Petsko, 1976; Walkinshaw et al., 1980; Love & Stroud, 1986; Basus et al., 1988; Labhardt et al., 1988). That is, the amide proton exchange rates, coupling constants, NOE constraints, and disulfide bonds suggest that the protein consists of three loops with a central triple-stranded antiparallel β sheet. In contrast to most other α-neurotoxins, however, nBgt exists as a dimer in solution [Chiappinelli & Lee (1985) and the present study]. Both NOE connectivities and proton exchange data are consistent with the dimeric form of the protein and indicate the position of the dimer interface. A similar pattern of dimerization deduced from NOE data has been observed for interleukin-8 (Clore et al., 1989, 1990). Like nBgt, the monomer of interleukin-8 contains an antiparallel β sheet. The dimer interface is at one edge of the β sheet, giving rise to a continuous six-stranded antiparallel β sheet in the dimeric structure.

Comparison between αBgt and nBgt. Despite the obvious differences in biological activity, αBgt and nBgt exhibit considerable structural similarity. The antiparallel β sheet found in nBgt is very similar to that observed for αBgt in solution. One possible exception is the lack of a hydrogen bond between the amide proton of Ile-20 and the carbonyl of Val-43 in nBgt, a position homologous to that of the hydrogen bond between the NH of Leu-22 and the carbonyl of Ala-45 in αBgt (Basus et al., 1988). The exchange rate of the Ile-20 amide proton is rapid, and no NOE peak was observed between NH of Ile-20 and NH of Val-43. This suggests that the β sheet is one hydrogen bond shorter in nBgt. The other end of the β sheet is of considerable interest for two reasons: (**1**) the β sheet is shorter in the crystal state than in the solution state for αBgt and (**2**) the tryptophan that is found in all neurotoxins except nBgt is found in this portion of the β sheet. As in the solution structure of αBgt, an NOE is present between the α protons of Ala-25 and Ile-38 (Met-27 and Val-40 in αBgt). In the crystal structure of αBgt, the α protons of Met-27 and Val-40 are separated by more than 10 Å. A small difference is observed between nBgt and αBgt concerning the contacts between Ser-55 and Ala-25/Gln-26 (Glu-56 and Met-27/Trp-28 in αBgt). The amide proton exchange rate is slow in nBgt for Ser-55, suggesting a possible hydrogen bond with the carbonyl oxygen of Ala-25. A corresponding hydrogen bond is not observed in αBgt. On the other hand, an NOE is observed between the NH of Glu-56 and the αCH of Trp-28 in αBgt is not observed for the corresponding nBgt residues. Nevertheless, preliminary structural calculations using distance geometry, homology model building, and restrained molecular dynamics (M. Sutcliffe et al., unpublished observations) for nBgt suggest that the side chain of Gln-26 is on the same side of the β sheet as Trp-28 in αBgt in solution (Inagaki et al., 1985; Basus et al., 1988) and opposite that of the crystal structure for αBgt (Love & Stroud, 1986). Thus, in this region of the β sheet, nBgt has a structure similar not only to the solution structure for αBgt but also to the crystal structure for other α-neurotoxins (Low et al., 1976; Tsernoglou & Petsko, 1976; Walkinshaw et al., 1980).

Although in solution αBgt exists as a monomer, in the crystal state it forms a dimer (Love & Stroud, 1986). The noncrystallographic dimer interface of αBgt is in the same region of the protein as nBgt and, like nBgt, forms a double-stranded antiparallel β sheet. Likewise, taking β sheets of both monomers into account, both crystalline αBgt and nBgt in solution form a six-stranded antiparallel β sheet. The extent of the intermolecular β sheet seems to be greater in nBgt than in crystalline αBgt, possible accounting for its persistence in solution. For αBgt, the contacts are between residues 57 and 59 (i.e., Val-57, Thr-58, and Cys-59), which corresponds to residues 56–58 of nBgt. For nBgt, the intermolecular contacts extend from Ser-55 to Cys-59. A related cardiotoxin from *Naja mossambica mossambica* also forms a noncrystallographic dimer (Rees et al., 1987) but is a monomer in solution.

In addition to the structural similarities of nBgt and αBgt, the chemical shifts of the amide and α protons for corresponding residues are highly correlated (Figure 7). In particular, NH and αCH protons arising from residues that are exactly conserved ($\oplus$) show remarkably similar chemical shifts in the two proteins. For example, the NH and αH protons of the three glycines in nBgt have chemical shifts very similar to those in the corresponding residues of αBgt (difference of 0.1 ppm or less for NH resonances and 0.24 ppm or less for αH resonances). With the exception of Ser-9 and Asn-65, all of the amide and α protons from residues in nBgt that are identical with those of αBgt resonate within 0.5 ppm of the corresponding proton in αBgt. This may suggest that comparisons with homologous proteins could be used to aid in the process of sequence-specific assignment (Redfield & Dobson, 1990).

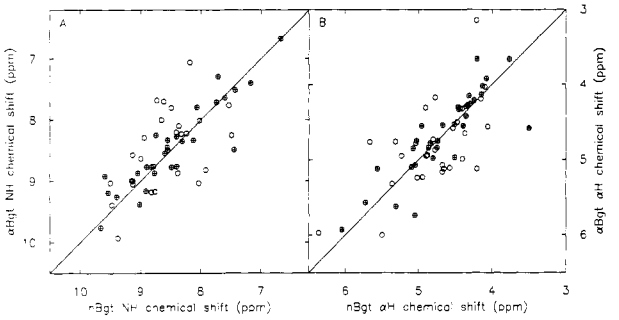

FIGURE 7: Comparison between the chemical shifts for the amide protons (A) and the α protons (B) of αBgt vs nBgt. All residues except those corresponding to deletions in the other protein are shown (i.e., Ile-11 and Ser-12 of αBgt and Phe-49 in nBgt are not shown; see Figure 1). (⊕) indicates residues that are exactly conserved and O represents those that are not.

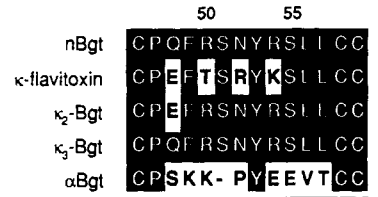

FIGURE 8: Comparison of the sequences of four neuronal α-neurotoxins and αBgt in the region that forms the dimer interface in the neuronal α-neurotoxins. The numbering is that for nBgt. The underlined region (Ser-55–Cys-59) represents the major point of contact between the two monomers in the dimer, and the orientation of the strand from Pro-47 to Ser-51 is crucial to dimer formation. Residues identical with those in nBgt are shown with a black background. Sequence information was obtained as follows: nBgt (Grant & Chiappinelli, 1885; Loring et al., 1986), κ-flavitoxin (Grant et al., 1988); κ_2- and κ_3-bungarotoxin (Danse & Garnier, 1990); and αBgt (Ohta et al., 1987; Kosen et al., 1988).

Comparison with Other Neuronal α-Neurotoxins. Chiappinelli et al. (1987) have isolated a peptide homologous to nBgt from the venom of *Bungarus flaviceps* (κ-flavitoxin) and two peptides homologous to nBgt from the venom of *B. multicinctus* captured in the Guangdong province of mainland China (κ_2-bungarotoxin and κ_3-bungarotoxin; Chippinelli et al., 1990). In addition, κ_2- and κ_3-bungarotoxins have been cloned and sequenced (Danse & Garnier, 1990). The venom of snakes containing κ_2- and κ_3-bungarotoxin does not contain nBgt. These toxins all have the same biological specificity as nBgt and form dimers in solution. Any combination of two of the four neuronal toxins is capable of forming heterodimers in a 1:2:1 ratio of homodimer:heterodimer:homodimer (Chiappinelli et al., 1989). The β strand forming part of the dimer interface (Ser-55–Cys-59) is exactly conserved in all four neuronal α-neurotoxins (Figure 8) and differs considerably from αBgt and other long α-neurotoxins that do not form dimers in solution (Karlsson, 1979). The other major consideration in dimer formation is the position of the strand from Pro-47 to Ser-51 in nBgt. In order to form a dimer, this strand must be out of the plane of the β sheet. This region also shows considerable homology between the four neuronal α-neurotoxins but differs considerably from other α-neurotoxins. In particular, the neuronal α-neurotoxins have an insertion of a Ser at position 51 (nBgt numbering) that is not present in other short and long α-neurotoxins. These sequence differences may account for the tendency of neuronal α-neurotoxins to form stable dimers in solution.

In conclusion, most of the sequence-specific ^{1}H NMR assignments have been made for neuronal bungarotoxin. On the basis of the NOE constraints, hydrogen exchange data, and coupling constants, the toxin has been shown to consist of a three-looped structure with a central triple-stranded antiparallel β sheet. The toxin forms a dimer with its interface along one edge of the triple-stranded β sheet, which in turn forms a six-stranded intermolecular β sheet.

ACKNOWLEDGMENTS

We thank Drs. Christina Redfield and Johnathan Boyd (Oxford Centre for Molecular Sciences) for extremely valuable advice and assistance throughout all phases of this project and Dr. Lu Yan Lian (Biological NMR Centre, Leicester, U.K.) for helpful discussions and assistance. We are grateful to Chaoying Zhang for performing the analytical ultracentrifugation measurements and to George Van Horn of Biotoxins, Inc., for the loan of nBgt.

REFERENCES

Aue, W. P., Bartholdi, E., & Ernst, R. R. (1976) *J. Chem. Phys. 64*, 2229–2246.
Basus, V. J., Billeter, M., Love, R. A., Stroud, R. M., & Kuntz, I. (1988) *Biochemistry 27*, 2763–2771.
Bax, A., & Davis, D. G. (1985) *J. Magn. Reson. 65*, 355–360.
Bax, A., & Drobny, G. P. (1985) *J. Magn. Reson. 61*, 306–320.
Bax, A., & Freeman, R. (1981) *J. Magn. Reson. 44*, 542–561.
Boulter, J., Connolly, J., Deneris, E., Goldman, D., Heinemann, S., & Patrick, J. (1987) *Proc. Natl. Acad. Sci. U.S.A. 84*, 7763–7767.
Braswell, E. (1968) *Biochim. Biophys. Acta 158*, 103–116.
Chazin, W. J., Kördel, J., Drakenberg, T., Thulin, E., Brodin, P., Grundström, T., & Forsén, S. (1989) *Proc. Natl. Acad. Sci. U.S.A. 86*, 2195–2198.
Chiappinelli, V. A. (1983) *Brain Res. 277*, 9–22.
Chiappinelli, V. A. (1984) *Trends Pharmacol. Sci. 5*, 425–428.
Chiappinelli, V. A., & Zigmond, R. E. (1978) *Proc. Natl. Acad. Sci. U.S.A. 75*, 2999–3003.
Chiappinelli, V. A., & Lee, J. C. (1985) *J. Biol. Chem. 260*, 6182–6186.
Chiappinelli, V. A., & Wolf, K. M. (1989) *Biochemistry 28*, 8543–8547.
Chiappinelli, V. A., Wolf, K. M., DeBin, J. A., & Holt, L. (1987) *Brain Res. 402*, 21–29.
Chiappinelli, V. A., Wolf, K. M., Grant, G. A., & Chem, S.-J. (1990) *Brain Res. 509*, 237–248.
Clore, G. M., Appella, E., Yamada, M., Matsushima, K., & Gronenborn, A. M. (1989) *J. Biol. Chem. 264*, 18907–18911.
Clore, G. M., Appella, E., Yamada, M., Matsushima, K,. & Gronenborn, A. M. (1990) *Biochemistry 29*, 1689–1696.
Cohn, E. J., & Edsall, J. T. (1943) *Proteins, Amino Acids and Peptides*, pp 370–381, Reinhold Publishing Corp., New York.
Danse, J.-M. & Garnier, J.-M. (1990) *Nucleic Acids Res. 18*, 1050.
Duvoisin, R. M., Deneris, E. S., Patrick, J., & Heinemann, S. (1989) *Neuron 3*, 487–496.
Eich, G., Bodenhausen, G., & Ernst, R. R. (1982) *J. Am. Chem. Soc. 104*, 3731–3732.
Endo, T., Inagaki, F., Hayashi, K., & Miyazawa, T. (1981) *Eur. J. Biochem. 120*, 117–124.
Evans, P. A., Kautz, R. A., Fox, R. O., & Dobson, C. M. (1989) *Biochemistry 28*, 362–370.
Grant, G. A. Frazier, M. W., & Chiappinelli, V. A. (1988) *Biochemistry 27*, 3794–3798.
Halvorsen, S. W., & Berg, D. K. (1987) *J. Neurosci. 7*, 2547–2555.

Inagaki, F., Hider, R. C., Hodges, S. J., & Drake, A. F. (1985) *J. Mol. Biol. 183*, 575–590.
Jeener, J., Meier, B. H., Bachmann, P., & Ernst, R. R. (1979) *J. Chem. Phys. 71*, 4546–4553.
Karlsson, E. (1979) in *Snake Venoms* (Lee, C. Y., Ed.) Handbook of Experimental Pharmacology 52, pp 159–212, Springer, Berlin.
Kline, A. D., Braun, W., & Wüthrich, K. (1988) *J. Mol. Biol. 204*, 675–724.
Kosen, P. A., Finer-Moore, J., McCarthy, M. P., & Basus, V. J. (1988) *Biochemistry 27*, 2775–2781.
Kumar, A., Ernst, R. R., & Wüthrich, K. (1980) *Biochem. Biophys. Res. Commun. 95*, 1–6.
Labhardt, A. M., Hunziker-Kwik, E. H., & Wüthrich, K. (1988) *Eur. J. Biochem. 177*, 295–305.
Loring, R. H., & Zigmond, R. (1988) *Trends Pharmacol. Sci. 11*, 73–78.
Loring, R. H., Chiappinelli, V. A., Zigmond, R. E., & Cohen, J. B. (1984) *Neuroscience 11*, 989–999.
Loring, R. H., Andrews, D., Lane, W., & Zigmond, R. E. (1986) *Brain Res. 385*, 30–37.
Love, R. A., & Stroud, R. M. (1986) *Protein Eng. 1*, 37–46.
Low, B. W., Preston, H. S., Sato, A., Rosen, L. S., Searl, J. E., Rudko, A. D. & Richardson, J. S. (1976) *Proc. Natl. Acad. Sci. U.S.A. 73*, 2991–2994.
Marion, D. & Wüthrich, K. (1983) *Biochem. Biophys. Res. Commun. 113*, 967–974.
McLane, K. E., Tang, E., & Conti-Tronconi, B. M. (1990) *J. Biol. Chem. 265*, 1537–1544.
Otting, G., & Wüthrich, K. (1987) *J. Magn. Reson. 75*, 546–549.
Pardi, A., Billeter, M., & Wüthrich, K. (1984) *J. Mol. Biol. 180*, 741–751.
Press, W. H., Flannery, B. P., Teukolsky, S. A., & Vetterling, W. T. (1986) *Numerical Recipes: The Art of Scientific Computing*, Cambridge University Press, New York.
Ravdin, P. M., & Berg, D. K. (1979) *Proc. Natl. Acad. Sci. U.S.A. 76*, 2072–2076.
Redfield, C., & Dobson, C. M. (1988) *Biochemistry 27*, 122–136.
Redfield, C., & Dobson, C. M. (1990) *Biochemistry 29*, 7201–7214.
Rees, B., Samama, J. P., Thierry, J. C., Gilibert, M., Fischer, J., Schweitz, H., Lazdunski, M., & Moras, D. (1987) *Proc. Natl. Acad. Sci. U.S.A. 84*, 3132–3136.
States, D. J., Haberkorn, R. A., & Ruben, D. J. (1982) *J. Magn. Reson. 48*, 286–292.
Tsernoglou, D., & Petsko, G. A. (1976) *FEBS Lett. 68*, 1–4.
Wagner, G., Wüthrich, K., & Tschesche, H., (1978) *Eur. J. Biochem. 86*, 67–76.
Walkinshaw, M. D., Saenger, W., & Maelicke, A. (1980) *Proc. Natl. Acad. Sci. U.S.A. 77*, 2400–2404.
Wüthrich, K. (1986) *NMR of Proteins and Nucleic Acids*, John Wiley & Sons, New York.
Yphantis, D. A., & Arakawa, T., (1987) *Biochemistry 26*, 5422–5427.

Glycophorin-Induced Cholesterol–Phospholipid Domains in Dimyristoylphosphatidylcholine Bilayer Vesicles†

R. Tampé, A. von Lukas, and H.-J. Galla*,‡
Institute of Biochemistry, Technical University Darmstadt, Petersenstrasse 22, D-6100 Darmstadt, FRG
Received November 7, 1990; Revised Manuscript Received February 8, 1991

ABSTRACT: Glycophorin has been incorporated into unilamellar cholesterol-containing dimyristoylphosphatidylcholine vesicles that were reconstituted by the freeze and thaw technique. Evidence was obtained for a protein-induced structural reorganization of these mixed membranes. By differential scanning calorimetry, we were able to construct a phase diagram for the phospholipid/cholesterol mixture consisting of a liquid-ordered, a solid-ordered, and a liquid-disordered phase. Glycophorin at low molar fractions ($X_G < 3 \times 10^{-3}$) increases the relative amount of lipid in the liquid-ordered phase, which is interpreted as an enrichment of cholesterol in the vicinity of the protein. The formation of such steroid-enriched domains could be demonstrated directly by electron paramagnetic resonance using a spin-labeled cholesterol analogue. A drastic increase of the spin–spin interaction of the labeled steroid was observed in the presence of glycophorin.

Cholesterol is a major component of all eucaryotic membranes, where this ubiquitous amphiphilic sterol amounts up to a mole fraction of $X_{Ch} = 0.5$ with respect to the total lipid. Its interaction with phospholipids has been the subject of numerous studies leading to a large number of different and sometimes controversial models that try to explain the thermodynamic properties of cholesterol-containing membranes. However, different experimental techniques appear to yield different results for the miscibility of phospholipids and cholesterol or for their association stoichiometry. Suggestions have been given for the construction of phase diagrams with phase boundaries at $X_{Ch} = 0.2$ (Shimshick & McConnell, 1973; Copeland & McConnell 1980; Melchior et al., 1980), at $X_{Ch} = 0.33$ (Engelman & Rothmann, 1972; Gershfeld, 1978; Lentz et al., 1980), at $X_{Ch} = 0.4$ (Kroon et al., 1975), and at $X_{Ch} = 0.5$ (Engelman & Rothmann, 1972). Phase boundaries at

† Supported by the Deutsche Forschungsgemeinschaft, Grant SFB 169/B2.
* To whom correspondence should be addressed.
‡ Present address: Institute of Biochemistry, University of Münster, Wilhelm-Klemm-Strasse 2, D-4400 Münster, FRG.

0006-2960/91/0430-4909$02.50/0